Sedimentology (2008) **55,** 667–687 doi: 10.1111/j.1365-3091.2007.00917.x

Sediment trend models fail to reproduce small-scale sediment transport patterns on an intertidal beach

GERHARD MASSELINK*, DANIEL BUSCOMBE*, MARTIN AUSTIN†, TIM O'HARE† and PAUL RUSSELL†
*School of Geography, University of Plymouth, Plymouth, UK (E-mail: daniel.buscombe@plymouth.ac.uk)
†School of Earth, Ocean and Environmental Sciences, University of Plymouth, Plymouth, UK

ABSTRACT

A rigorous test is presented of the application of sediment trend models to an intertidal beach environment characterized by bar morphology. Sediment samples were collected during low tide from a regular grid and their sediment fall velocity distributions, obtained using a settling tube, were analysed using moment analysis. The net sediment transport direction determined from beach surveys, hydrodynamic measurements, wave ripple observations and sediment transport modelling was compared with predictions by sediment trend models based on the spatial distribution of sediment parameters. It was found that the sediment transport pathways and patterns of sedimentation predicted using sediment trend models were at odds with field observations, and varied significantly depending on whether surface or sub-surface sediment samples were used. The sediment trend models are thought to fail because, in energetic and morphologically variable beach environments, spatial patterns in sediment characteristics are mainly attributed to the presence of different hydrodynamic regions and associated morphology, rather than sediment pathways. The use of sediment trend models cannot replace the collection of morphological, hydrodynamic and sediment transport data in the field to define relationships between flows, forms and sedimentation patterns on a dynamic intertidal beach.

Keywords Beach morphology, hyperbolic triangle, log-hyperbolic distribution, nearshore sediment transport, particle analysis, sediment trend models.

INTRODUCTION

The textural characteristics of beach sediments are not constant, but change substantially over space and in time (e.g. Masselink *et al.*, 2006). This is an important observation, because sediment size plays a crucial role in sediment transport processes and, hence, morphological change. The sediment transport rate is linked directly to the bed shear stress through the quadratic stress law (or a variation thereof), which takes account of both the flow velocity and the roughness of the sea bed controlled by the sediment size (Van Rijn, 1993). Once a sediment particle is suspended, its fate strongly depends on the sediment fall velocity. Because the spatial and temporal variability of beach sediment characteristics are generally poorly understood, a constant sediment size often is assumed. This assumption represents a major limiting factor in models of beach change (e.g. Soulsby, 1997), because the errors introduced into morphodynamic models of beaches due to uncertainties in grain parameters and/or the use of a single time/space-averaged sediment size value may be significant. A consideration of changes in grain size may, in fact, improve the output of models of nearshore change, such as demonstrated by Gallagher *et al.* (1998) in their modelling of sand bar migration.

Early studies emphasized that textural variability in beach environments may be due to different hydrodynamic processes acting on different portions of the profile (Bascom, 1951; Inman, 1953; Miller & Ziegler, 1958), resulting in textural

© 2007 The Authors. Journal compilation © 2007 International Association of Sedimentologists

differences between various secondary morphological features (such as berm, cusp, beach step, bar, etc.) superimposed upon the primary beach profiles. For example, it is well-established that the beach step is the coarsest and most poorly sorted sediment unit of reflective beaches (Bauer & Allen, 1995). The beach step derives its distinctive sedimentological signature from the presence of energetic breaking wave conditions, which tend to concentrate the coarsest sediment fractions. Similarly, nearshore bars are generally characterized by coarser and better-sorted sediments than associated troughs (Greenwood & Davidson-Arnott, 1972; Van Houwelingen *et al.*, 2006). The persistent breaking of waves on the bar surface tends to remove the finer sediment fractions, which end up in the relatively quiescent trough. Here these fine sediments mix with the antecedent sediment, resulting in an overall finer, but more poorly sorted, sediment distribution. The opposite can also be the case, where strong currents and/or intense wave stirring in channels may result in the formation of a coarser, poorly sorted lag deposit (Mothersill, 1969). A final extreme example of the development of different sediment facies on beaches is found on coarse-grained beaches subjected to large tidal ranges, where a coarse-grained, steep upper intertidal zone is often found separated by a distinct break in slope from a finer-grained, low-tide terrace (Short, 1991; Masselink & Short, 1993; Turner, 1995).

Sediment sorting processes operate during all stages of sediment transport, including entrainment, transport and deposition (Slingerland, 1977; McLaren, 1981; Hughes *et al.*, 2000), and sorting generally improves in the direction of sediment transport. To apply this notion in reverse, spatial patterns in beach sediment characteristics can be interpreted in terms of sediment transport processes. Specifically, the models based on this premise of McLaren & Bowles (1985), Gao & Collins (1992) and Le Roux (1994) have been applied to beach environments to derive sediment pathways from spatial patterns in sediment characteristics (Pedreros *et al.*, 1996). Additionally, Barndorff-Nielsen & Christiansen (1988) propose that patterns of erosion and accretion are imprinted upon the sedimentology, and this model also has been applied to beaches (Hartmann & Christiansen, 1992; Sutherland & Lee, 1994). Using spatial patterns in the sediment characteristics to determine sediment pathways represents an attractive alternative to using conventional methods, which involve the deployment of vast arrays of expensive instrumentation and/or sophisticated numerical modelling.

The objective of this paper was to investigate to what extent the variability in sediment characteristics across the intertidal region of a mesotidal, high-energy, medium-sand beach reflects secondary morphological features, sediment transport pathways and erosion/accretion patterns. Sediment transport pathways are defined here as the spatial pattern of the net sediment transport direction across the intertidal zone that has occurred over a single tidal cycle. In addition to conducting a thorough and objective test of the sediment trend models of Barndorff-Nielsen & Christiansen (1988) and Gao & Collins (1992), the novel aspect of this paper is that, rather than using the sediment size distribution to compute the sediment parameters, the sediment fall velocity distribution is used. To provide a proper morphodynamic context for the sediment data, the first part of the paper provides a general description of the morphological response of the beach over a spring-to-spring tidal cycle and a detailed discussion of the hydrodynamic processes across the intertidal region during a single tidal cycle. In the second part of the paper, the results of the sediment analysis and the testing of the sediment trend models are presented.

METHODOLOGY

Field site

A field campaign was held over a spring-to-spring tidal cycle in May 2006 on Truc Vert beach, France (Fig. 1). The beach experiences a mean spring tide range of 4·3 m and is subjected to an energetic wave climate of prevailing westerly swell with an average significant wave height of 1·3 m and typical significant wave heights during storms of 5 m (De Melo Apoluceno *et al.*, 2002). A subtidal crescentic bar system protects the intertidal beach from exposure to such extreme wave conditions and inshore significant wave heights are generally less than 2·5 m, even during spring high tide. The median sediment size D_{50} on the beach is typically around 0·35 mm.

Beach morphology

At the start of the field campaign, three cross-shore transects, spaced 20 m apart, were established. The transects, at $y = -40$ m, -20 m and 0 m (Fig. 2), started at the foot of the foredunes

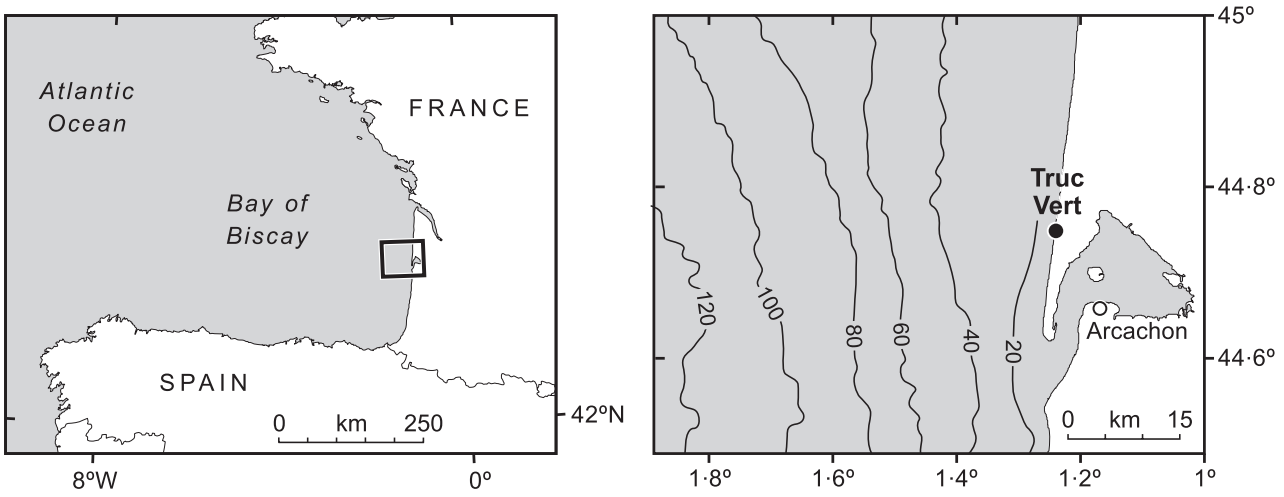

Fig. 1. Location of the study area.

and extended across the intertidal region as far as the mean low water level. The beach morphology at these transects was measured every low tide using a total station (vertical accuracy of the order of millimetres) from 8 May (Tide 1) to 23 May (Tide 31). A much larger region of the beach was surveyed every few days using differential GPS (vertical accuracy of the order of centimetres). The beach morphology during the first part of the field campaign, when wave conditions were relatively calm, is shown in Fig. 2 and is representative of summer conditions, characterized by a steep upper beach and a pronounced berm. The mid-to-lower intertidal region has a much gentler gradient and is characterized by intertidal bar-rip morphology. The bar is very subdued and is perhaps better described as a terrace; it is located in the centre of the survey grid and subdued rip channels and present at the southern and northern ends of the grid.

Nearshore hydrodynamics and sediment transport

Nearshore hydrodynamics were measured at five locations across the bar-trough morphology along the cross-shore transect $y = -20$ m (at $x = 100$, 110, 120, 130 and 140 m; Rigs 1 to 5). At each location, a Druck pressure transducer (PT) (Keller AG, Winterthur, Switzerland) was used to measure waves, the nearshore flow field was recorded using Valeport electromagnetic current meters (ECM) (Valeport Limited, Totnes, UK) and Nortek acoustic Doppler velocimeters (ADV) (Nortek AS, Rud, Norway) deployed 0·15 m from the bed, and Downing optical backscatter sensors (OBS) (D&A Instrument Company, Port Townsend, WA, USA) were used to measure suspended sediment concentrations (also at 0·15 m from the bed). At location $x = 130$ m (Rig 4), a vertical array of custom-built mini-OBS sensors was installed to record the vertically integrated suspended sediment flux. Unfortunately, these data are only useful when collected at night; during the day, the ambient sunlight causes saturation of the output signal of the mini-OBS sensors. Data were recorded at 4 Hz and were recorded internally or logged on a shore-based computer. Two sand ripple profilers (SRP) (Marine Electronics, Guernsey, UK) were installed along the same transect at $x = 110$ and 130 m to monitor the bed morphology. The SRPs were set to scan a 2 m wide section of the sea bed every minute to record the bed-level profile at millimetre-accuracy and these data were used to give information on wave ripple geometry and migration. The acoustic SRP devices do not give reliable information on the sea bed morphology when they are subjected to energetic breaker waves and only the SRP data collected at $x = 110$ m are used here. More information on the instrumentation used is given in Tinker *et al.* (2006) and Austin *et al.* (2007). To complement the nearshore hydrodynamic data, offshore wave conditions were provided by the French Navy (Ardhuin *et al.*, 2007) using a calibrated model output for a point in 55 m water depth (44°39′ N; 1°27′ W).

Nearshore hydrodynamic data were collected every low tide from 9 May (Tide 3) to 21 May 2006 (Tide 26) but, for the present paper, only the data recorded on 19 May (Tide 22) will be discussed. Statistical analysis on the hydrodynamic time series was conducted using 20 min data sections. For each of these, the following

© 2007 The Authors. Journal compilation © 2007 International Association of Sedimentologists,

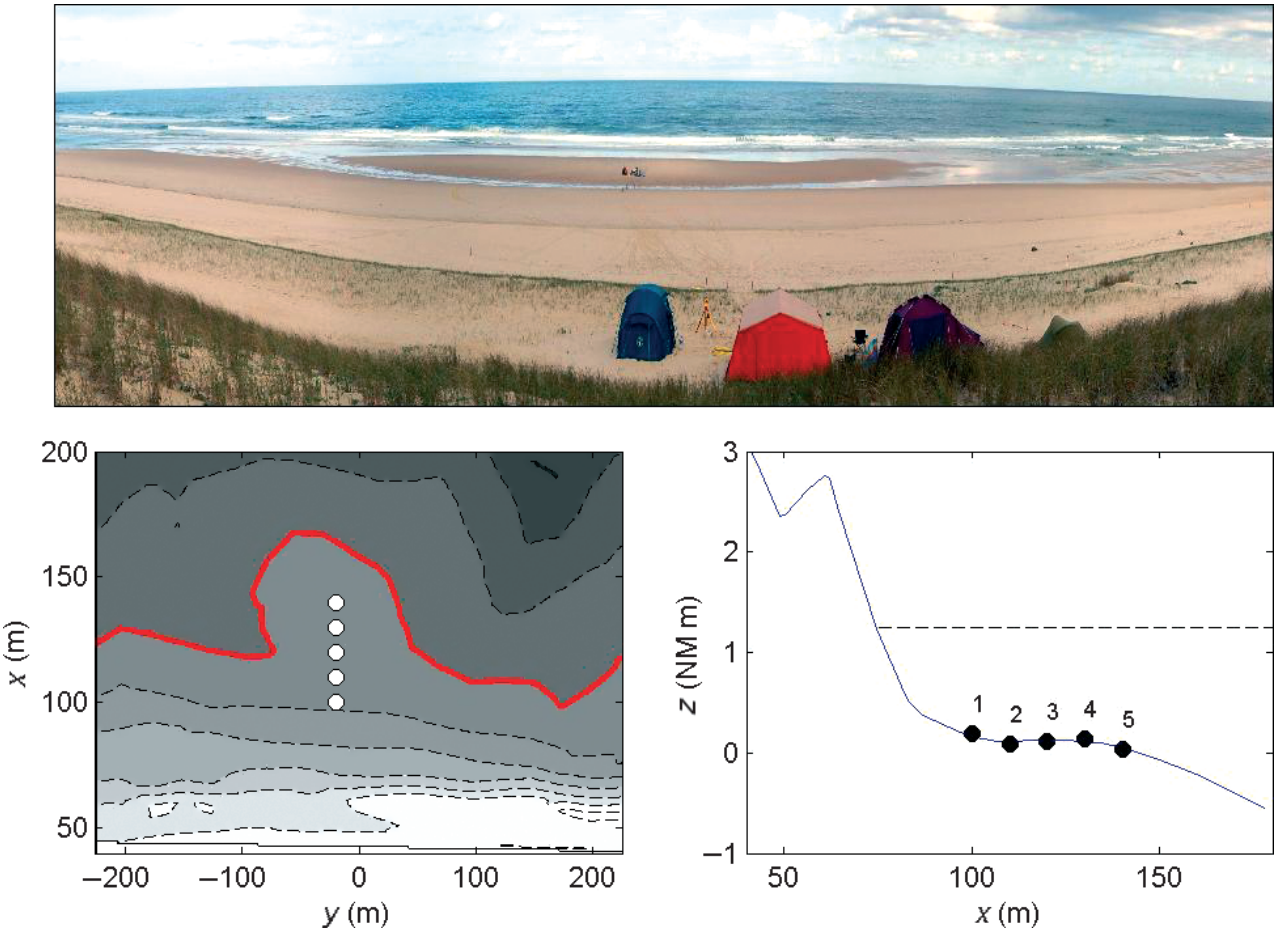

Fig. 2. Upper panel: photo mosaic taken at the start of the field campaign at low tide with the instrument transect going through the middle of the image across the intertidal bar (photograph by Tim Scott). Bottom left panel: three-dimensional beach morphology measured using differential GPS on 14 May 2006. The white circles show the instrument locations and the rectangle represents the sediment sampling grid. The colour axis runs from +3 m (white) to −1 m (dark grey) and the survey datum is Niveau Moyen (NM), which is approximately mean sea-level in France. The thick contour line represents 0 m NM. Bottom right panel: beach profile measured with total station at $y = -20$ m on 19 May 2006 and the horizontal line represents the mean water level attained during high tide on that day. The black circles show the instrument locations (Rigs 1 to 5).

parameters were computed: mean water depth h, significant wave height H_s (computed as $4\eta_\sigma$, where η_σ is the standard deviation of the water surface elevation record), significant wave period T_s (computed as m_0/m_1, where m_0 and m_1 are, respectively, the zeroth and first moment of the wave spectrum), mean cross-shore current $<u>$, maximum wave orbital velocity U_m (computed as $2u_\sigma$, where u_σ is standard deviation of the cross-shore current record u) and mean longshore current $<v>$.

To complement the standard hydrodynamic parameters, two additional sediment transport parameters were derived. The Shields parameter θ was used to represent the non-dimensional bed shear stress according to:

$$\theta = \frac{0{\cdot}5 f_w U_m^2}{(s-1) g D_{50}} \quad (1)$$

where s is the ratio of the densities of sediment and sea water ($\rho_s = 2650$ kg m^{-3}; $\rho = 1000$ kg m^{-3}), g is gravity ($g = 9{\cdot}8$ m s^{-2}) and f_w is a wave friction factor which, following Swart (1974), can be approximated as:

$$f_w = \exp\left[5{\cdot}213\left(\frac{k_s}{A}\right)^{0{\cdot}194} - 5{\cdot}977\right] \quad (2)$$

where k_s is the bed roughness given by $k_s = 2{\cdot}5 D_{50}$ (with $D_{50} = 0{\cdot}35$ mm) and A is the maximum bottom orbital semi-excursion given by

© 2007 The Authors. Journal compilation © 2007 International Association of Sedimentologists,

$A = U_m T_s/2\pi$. The net cross-shore sediment transport rate i was computed using the Bailard (1981) energetics equation according to:

$$i = i_b + i_s = \rho C_f \frac{\varepsilon_b}{\tan\phi}\left[|u|^2 u - \frac{\tan\beta}{\tan\phi}|u|^3\right] + \rho C_f \frac{\varepsilon_s}{w_s}\left[|u|^3 u - \frac{\varepsilon_s \tan\beta}{w_s}|u|^5\right] \quad (3)$$

where i is the immersed weight sediment transport rate, the subscripts 'b' and 's' indicate, respectively, bedload and suspended load, C_f is a friction coefficient ($C_f = 0{\cdot}003$), u is the cross-shore current velocity, w_s is the sediment fall velocity ($w_s = 0{\cdot}05$ m s^{-1}), ε is an efficiency factor ($\varepsilon_b = 0{\cdot}135$; $\varepsilon_s = 0{\cdot}015$), tan φ is the tangent of the internal angle of friction (tan $\varphi = 0{\cdot}63$) and tan β is the bed gradient (tan $\beta = 0{\cdot}03$). The values for the constants are taken from Gallagher *et al.* (1998) who applied Eq. (3) to simulate the migration of a subtidal bar. The volumetric transport rate q was derived from the immersed weight transport rate using:

$$q = \frac{i}{g(\rho_s - \rho)} \quad (4)$$

where q has units of m^3 s^{-1} per unit metre beach width (i.e. m^2 s^{-1}) and was converted to m^2 h^{-1} for convenience.

Sediment sampling and analysis

To provide a time series of sediment characteristics, a sediment sample was collected every low tide from the crest of the intertidal bar ($x = 130$ m; $y = -20$ m). Prior to sampling, the mixing depth (or depth of disturbance) was determined using the rod-and-washer method (Jackson & Nordstrom, 1993). A small plastic tube (diameter = 2·5 cm) was then pushed into the sand up to the mixing depth level and a sample was taken. In the morning of 19 May 2006, before Tide 22, a survey grid was established comprising 14 cross-shore transects spaced 20 m apart ($y = -150$–110 m) and six alongshore transects spaced 15 m apart ($x = 70$–145 m). The chosen spacing of the sediment sampling grid was close enough to ensure adjacent samples were likely to be related by the transport regime. At each transect intersection ($N = 84$), a 1·2-m long fibreglass rod was inserted into the bed and a washer was placed over it. The location and elevation of each point was surveyed using the total station. In the evening of 19 May, after Tide 22 had flooded and retreated, each grid point was re-surveyed and the mixing depth was determined through excavation of the washer. Two sediment samples were then collected at each grid point: (i) a scrape of the surface layer (<1 cm; referred to as the 'surface sample'); and (ii) a small sediment core representing the mixing depth (5 to 15 cm, depending on sample location; referred to as the 'sub-surface sample'). Two samples were taken at each location because previous work indicated that surface samples may not be representative of the active layer (Masselink *et al.*, 2006).

Beach sediment characteristics are traditionally analysed with sieves, yielding the sediment size distribution from which parameters such as mean size, sorting and skewness can be derived through various methods (Blott & Pye, 2001). A major problem with sieving is the rather coarse resolution of the sediment distribution, even when sieving at 1/4φ intervals. Laser sizers can be used to obtain an almost-continuous sediment size distribution but, even so, it is questionable whether size is the most relevant property of sediments in the intertidal zone from a sediment dynamic point of view. Swash and surf zone processes are highly energetic and the dominant mode of sediment transport is suspended transport. Under such a sediment transport regime, the fall velocity of a sediment particle is likely to be of more relevance than its size; therefore, the fall velocity distribution, rather than the size distribution, forms the basis for computing sediment parameters in the present investigation.

In the laboratory, a sub-sample of *ca* 5 g was obtained from all surface and sub-surface samples. Extreme care was taken to ensure that the sample was well-mixed prior to sub-sampling. Shell fragments were present in most samples and these were not removed, because they are an integral part of the beach sediment size distribution. The samples were analysed in random order using a settling tube with a diameter of 25 cm and a length of 2·5 m. A balance was installed above the tube with a plastic tray suspended from it at 2·2 m below the water surface using a thin fishing line. The cumulative weight on the tray was recorded by the balance at a resolution of 1 mg and logged on a computer at 2 Hz. Data recording started the moment the sample was introduced into the settling tube and was terminated when all sediment particles had settled on the tray at the bottom of the tube (usually within 2 min). The raw data of the settling tube is a two-column matrix of time (s) and weight (g), which is

© 2007 The Authors. Journal compilation © 2007 International Association of Sedimentologists,

converted easily to sediment fall velocity (m s^{-1}) and percentage weight.

Figure 3 shows the relative and cumulative frequency distribution of the sediment size (obtained through conventional sieving at 1/4φ intervals) and the fall velocity for a typical sample from Truc Vert. The difference in resolution is obvious and there is noticeably more detail at the tail ends of the fall velocity distribution compared with that of the sediment size. Both distributions have a positive skewness (i.e. fine-skewed) and this is most obvious in the fall velocity distribution.

Analogous to sediment size data analysis, when the grain diameter D in millimetres is transformed to phi-units using $\varphi = -\log 2(D)$, the fall velocity w_s was transformed to psi-units following Gibbs *et al.* (1971) using $\psi = -\log 2(w_s)$. Moment analysis was used to compute the mean fall velocity and the associated standard deviation (sorting) and skewness. The tails (2·5%) of the frequency distribution of ψ were removed prior to computing the moments, because the skewness parameter is overly sensitive to the tails, and the presence of only a few coarse sediment grains in the sample has a very large effect on the skewness. The particular method used to determine the grain-size parameters (moment analysis or Folk and Ward graphic method) and whether the tails are removed or not are not too important for sediment trend analysis, as the relative values between sampling points are more important than the absolute values (Le Roux and Rojas, in press).

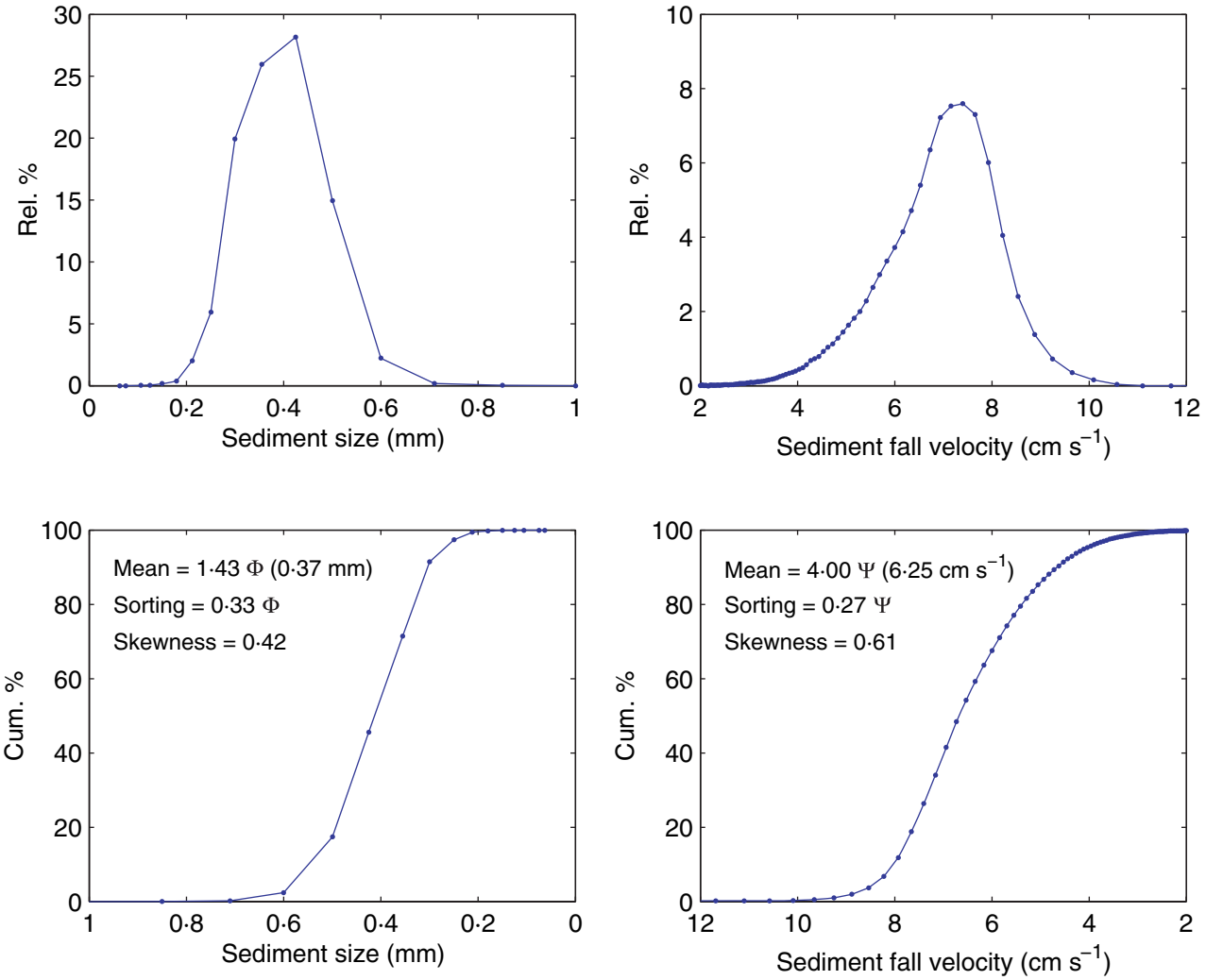

Fig. 3. Comparison of relative (top panels) and cumulative (bottom panels) frequency distributions of sediment size (left panels) and fall velocity (right panels) of a typical sample collected from Truc Vert. Note that the *x*-axes for the upper and lower panels are reversed.

When using small quantities of sediment for analysis, there is always the risk that a sub-sample is not representative of the bulk sample. To investigate this, 11 sub-samples were obtained from a single bulk and were dropped sequentially in the settling tube. The procedure of mixing and splitting the sample to obtain these sub-samples was identical to that used for the other samples. The average values for the mean fall velocity, sorting and skewness (dimensionless) were, 7·35 cm s^{-1} (0·06), 0·37 ψ (0·01) and −0·26 (0·05), respectively, where the numbers in parentheses represent the associated standard deviations.

Sediment trend analysis

Spatial changes in sedimentary parameters (size, sorting and skewness) have been used by several researchers to infer probable net sediment transport pathways, and there are several versions available (e.g. McLaren & Bowles, 1985; Gao & Collins, 1992; Le Roux, 1994; Lucio *et al.*, 2006; Poizot *et al.*, 2006). The method proposed by Gao & Collins (1992), henceforth referred to as the grain-size trend analysis (GSTA) model, is the most suitable method for the marine environment and is adopted here to be comparable directly with previous studies [being available as a commercial product/service, the model of McLaren & Bowles (1985) appears more widely used, but one of the main assumptions of the approach is that the sediment transport is by uni-directional currents].

According to the GSTA model of Gao & Collins (1992), in the direction of sediment transport, sediments may become either finer, better sorted and more negatively skewed (FB−; Case 1) or coarser, better sorted and more positively skewed (CB+; Case 2). These two sediment trends also are considered in the GSTA models of McLaren & Bowles (1985) and Le Roux (1994), where they are referred to as Case B and C, and Type 1 and 2, respectively. After comparing the sediment characteristics (size, sorting and skewness) of adjacent sample points, vectors of unit length are drawn between two points if they conform to the 'rules' of the GSTA model (i.e. FB− or CB+; cf. Gao, 1996). These vectors are calculated from every point with respect to the immediate eight neighbouring points, using a characteristic transport distance D_{cr} equal to the diagonal of the sampling grid, in this case 25 m. Summing the vectors at each sample point produces a single vector, which should reflect the net trends in sediment transport (i.e. the *trend* vector). Gao & Collins (1992) undertake two further steps in the analysis: (i) the trend vectors are averaged over the characteristic transport distance D_{cr} to remove noise and obtain *transport* vectors; and (ii) the significance of the transport vectors is tested based on the length of the vectors (long vectors are more significant than short vectors). These two additional steps are discussed later in the section headed *Sediment trend analysis*.

Gao & Collins (1991) mathematically described how two more sediment trends might occur (FB+ and CB−), a concept continued in the work of Le Roux *et al.* (2002). As hinted at by McLaren et al. (in press), an alternative sediment trend model therefore can be formulated solely based on the sediment sorting, whereby sediment trend vectors are drawn from the spatial gradient in sorting values (multiplied by −1, because an improvement in sorting is sought). In other words, the direction and length of the trend vectors at each of the sample locations are proportional to the first directional derivative of sorting, and the contributions of size and skewness are ignored. This model is referred to as the 'sorting model' and differs mainly from the GSTA model in that steep sorting gradients contribute more to the resulting sediment trend vectors than weak sorting gradients. In the present case with a regular grid, the sorting trend surface simply is determined through linear interpolation, but with an irregular grid more sophisticated kriging techniques will need to be implemented.

The log-hyperbolic shape triangle

Bagnold (1941, 1954) observed that in a natural log–log plot of grain-size distributions, the tails were 'heavy' compared to a normal distribution, and almost linear. Bagnold articulated that the normal distribution, with its fixed kurtosis and inherent symmetry, was often at odds with measured grain-size distributions, and thus conventional grain-size statistics (which assume normality) may be inadequate descriptors. Barndorff-Nielsen (1977) recognized that grain-size distribution characteristics were better approximated by a log-hyperbolic probability density function (a hyperbola controlled by four parameters $\mu,\delta,\varphi,\gamma$), rather than the traditional normal model (a parabola controlled by two parameters μ,σ).

The log-hyperbolic curve was introduced to the sedimentological community by Bagnold & Barndorff-Nielsen (1980) and is given by:

© 2007 The Authors. Journal compilation © 2007 International Association of Sedimentologists,

$$p(x;\mu,\delta,\phi,\gamma) = \frac{\sqrt{(\phi\gamma)}}{\delta(\phi+\gamma)} K_1(\delta\sqrt{(\phi\gamma)}) \times \exp\left\{\frac{-\delta}{2}\left[(\phi+\gamma)\left(1+\left(\frac{x-\mu}{\delta}\right)^2\right) - (\phi-\gamma)^{x-\mu/\delta}\right]^{1/2}\right\} \quad (5)$$

where K_1 is a first-order Bessel function. The parameter μ gives location [the peak diameter of Bagnold (1941)], δ provides scale [equivalent to the standard deviation of Folk & Ward (1957)], and φ and γ give the slopes of the left and right tails, respectively. The parameters of the log-hyperbolic distribution allow greater flexibility and improved model fit to observed distributions, as well as the derivation of further parameters which may be beneficial in sediment classification and physical interpretation of grain-size distributions (Hartmann & Christiansen, 1992). However, it has yet to be demonstrated convincingly that the use of log-hyperbolic grain-size statistics gives greater insights into the physical processes of sedimentation and sediment transport (e.g. Wyrwoll & Smyth, 1985). The ShefSize program (Robson *et al.*, 1997) was used here to fit the distributions to the measured settling velocity distributions.

Log-hyperbolic peakedness (kurtosis) and symmetry (skewness) are given by, respectively:

$$\xi = 1 + \delta\sqrt{(\phi\gamma)}^{-1/2} \quad (6)$$

and:

$$\chi = \left(\frac{\phi-\gamma}{\phi+\gamma}\right)\xi \quad (7)$$

and are invariant under transformations of scale and location. The domain of variation between ξ and χ is known as the hyperbolic shape triangle (Fig. 4). Log-normal distributions have non-heavy tails and rounded peaks at the mode, and plot near $\xi = 0$; log skew-Laplace distributions have heavy tails and sharp peaks near the mode, and plot near $\xi = 1$; and log-hyperbolic distributions have heavy tails and more rounded peaks near the mode, and plot near $\xi = 0{\cdot}5$. Barndorff-Nielsen & Christiansen (1988) presented a physical–mathematical model, from first principles, for the erosion and deposition of sand, where the [ξ, χ] position should move to the right of the shape triangle under erosion, and to the left under deposition. The assumption here is that the probability of the proportion of grains of a given size after an erosive period (relative to the proportion of those grains at the beginning of that period) is proportional to some power of that given size. This assumption has some physical plausibility because it has been demonstrated that thresholds of entrainment are governed by pow-

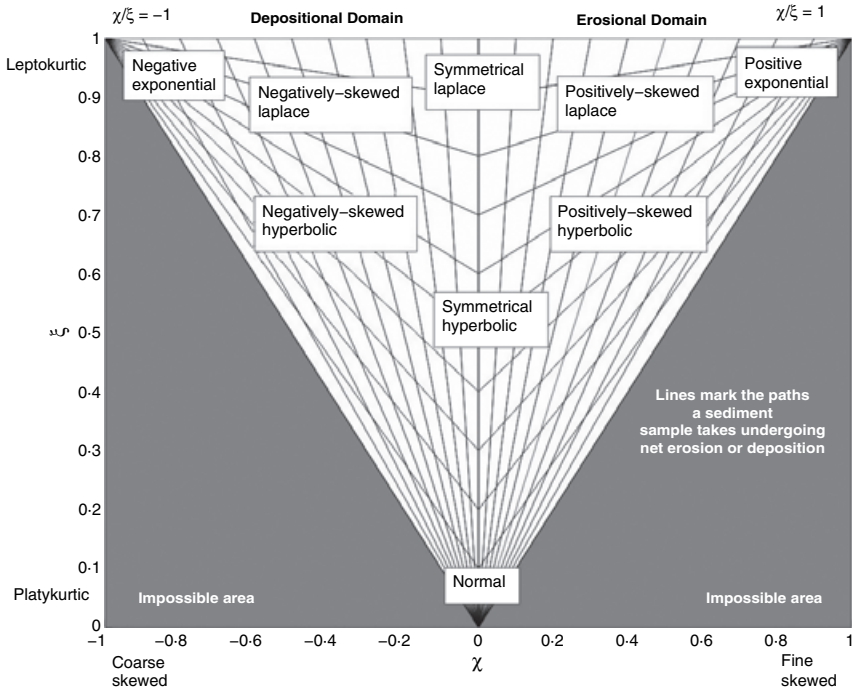

Fig. 4. The hyperbolic shape triangle of Barndorff-Nielsen & Christiansen (1988). The white and shaded triangular areas represent the possible and impossible domains, respectively, of the variation between [ξ, χ]. The left hand side of the shape triangle, towards $\xi/\chi = -1$, represents the 'depositional' domain, and the right hand side of the shape triangle, towards $\xi/\chi = 1$, the erosional domain. According to the model of Barndorff-Nielsen & Christiansen (1988), sediment samples undergoing net erosion or deposition have [ξ, χ] pairs which travel along the lines drawn within the shape triangle. The shape triangle is also useful as a classification tool: some limiting cases of the log-hyperbolic distribution are shown in their double-logarithmic form, including the normal, exponential and Laplace distributions.

ers of velocity (e.g. Bridge, 1981). Selective sorting processes are expressed as changes in distributional form; thus, under erosion and deposition, the shape position moves along specified curves within the triangle (Barndorff-Nielsen & Christiansen, 1988).

Grain proportions are taken by settling; therefore, the number of single particles is unknown and this lack of sample size negates the use of conventional measures of goodness-of-fit such as chi-square. The 'quasi sample size' statistic of Fieller *et al.* (1992) is adopted here:

$$N_{\text{crit}} = \frac{\chi^2_{t:0\cdot95}}{\sum_1^k r_i - p_i(\theta)^2 / p_i(\theta)} \quad (8)$$

where $t = k - m - 1$, k is the number of size classes and m is the number of parameters estimated by model θ. This measure accounts for model parsimony (degrees of freedom as a conditional factor in the numerator) and a lack of sample size, and is interpreted as the critical sample size required to detect a lack of model fit at the 5% level (Fieller *et al.*, 1992). The higher the value of N_{crit}, the better the distributional fit.

RESULTS

Event history

Figure 5 shows the offshore wave conditions and the beach morphological response during the field experiment on Truc Vert. Two distinct phases in wave forcing were experienced during the field survey: (i) a 10-day period with low and

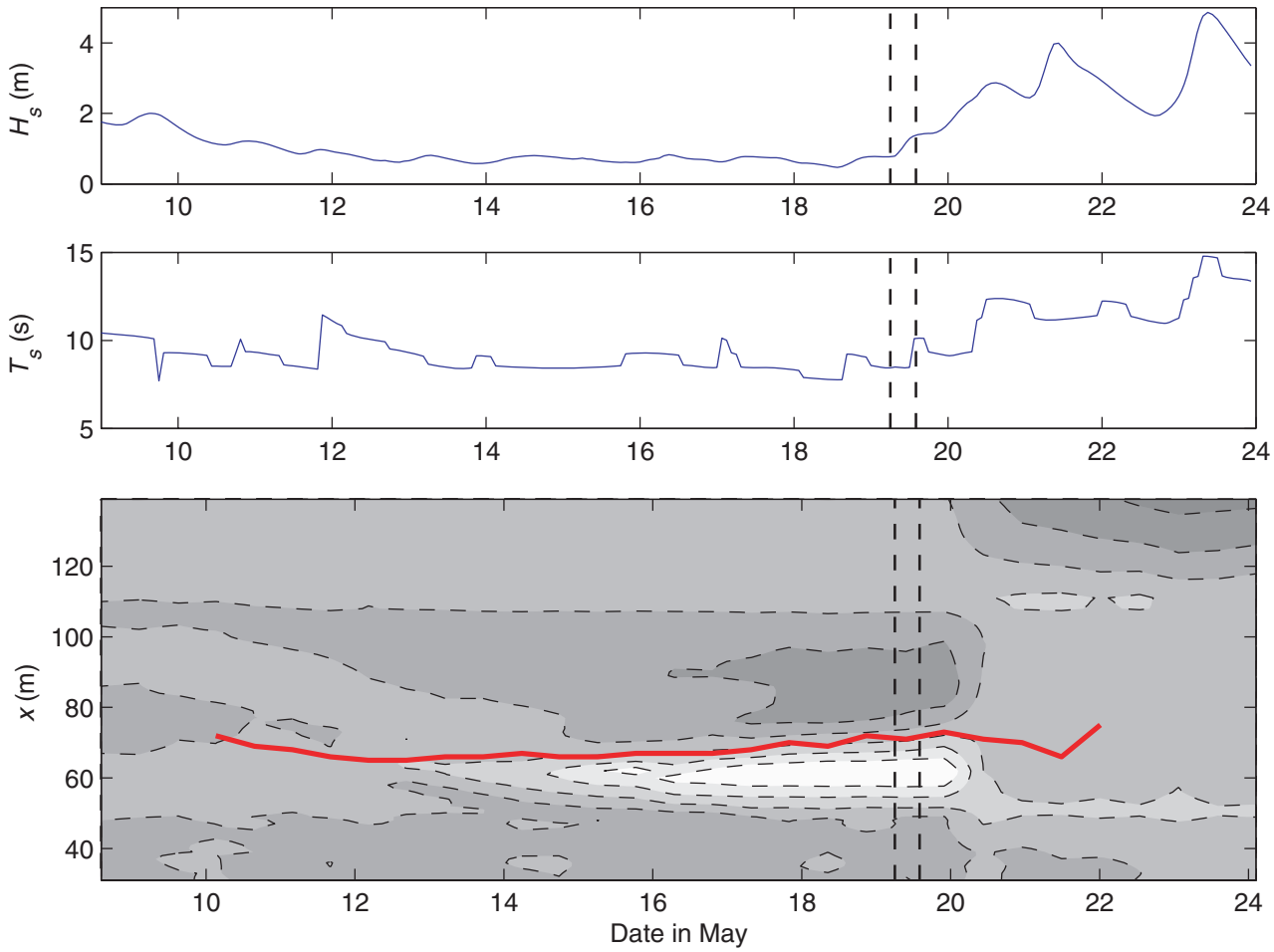

Fig. 5. Hydrodynamic forcing and intertidal beach response during the field campaign on Truc Vert in May 2006. Upper panel: offshore significant wave height. Middle panel: offshore significant wave period. Lower panel: intertidal morphology relative to the beach profile at the start of the measurement period (i.e. cumulative change) with the colour axis running from −0·6 m (grey) to +0·8 m (white). The thick solid line in the bottom panel represents the position of the high tide water level and the vertical dashed line indicates the tide during which sediment samples were taken for sediment trend analysis.

© 2007 The Authors. Journal compilation © 2007 International Association of Sedimentologists,

declining wave energy conditions characterized by H_s of 1 to 2 m and T_s of 10 s; and (ii) a 5-day period with high wave energy characterized by H_s of 2 to 5 m and T_s of 12 to 15 s. The morphological change data clearly show the progressive build-up of a pronounced swash bar under calm waves from 8 to 19 May 2006 due to onshore sediment transport from the inner part of the surf zone into the swash zone. During this period, the intertidal bar system remained stable and the only noticeable change was the infilling of the small trough. The complete swash bar system was destroyed during a single high tide on 20 May, hereafter referred to as Tide 23. Some of the swash bar sediment was pushed onshore into the runnel, but most of it was taken offshore, resulting in a planar concave beach profile that remained relatively stable despite the continuing exposure to high energy wave conditions. The tide during which the sediment samples were taken was the last one to be characterized by beach build-up; the proceeding tide resulted in the complete eradication of the berm feature. The fall velocity of the sediments at the crest of the bar ($x = 130$ m) progressively increased from 6 cm s^{-1} at the start of the field campaign to 6·5 cm s^{-1} at the end (not shown).

Morphological response during Tide 22

The morphological changes that occurred in the intertidal zone during Tide 22 were modest, but significant (Fig. 6). The upper beachface ($x = 60$ to 80 m) accreted, whilst the lower beachface ($x = 80$ to 100 m) eroded. The morphological change over the lower part of the profile was more three-dimensional but, in the central section ($y = -70$ to 30 m), onshore bar migration occurred, caused by erosion of the seaward slope of the bar and accretion of the bar crest and the landward slope of the bar. From the pattern of morphological change, an overall onshore sediment transport across the intertidal region can be deduced.

Hydrodynamics and sediment transport during Tide 22

The hydrodynamic conditions recorded at the five instrument locations during Tide 22 are controlled largely by the tide (Fig. 7). The temporal variation in h and H_s indicates that the wave height was depth-limited at all locations and throughout the tidal cycle; therefore, surf zone conditions prevailed and the high tide breakpoint was located seaward of the sampling grid. The prevalence of surf zone conditions is confirmed further by the observation that the highest wave heights are observed at Rig 5, and that the relative wave height H_s/h is consistently larger than 0·5 (cf. Thornton & Guza, 1982). Maximum wave heights of $H_s = 0{\cdot}8$ m were recorded during high tide at Rig 5.

The mean cross-shore and longshore currents in the surf zone are predominantly in the onshore and southward direction, respectively, and flow velocities are strongly modulated by the tide. The currents decrease in strength with increasing water depth and maximum cross-shore and longshore flow velocities are 0·25 and 0·4 m s^{-1},

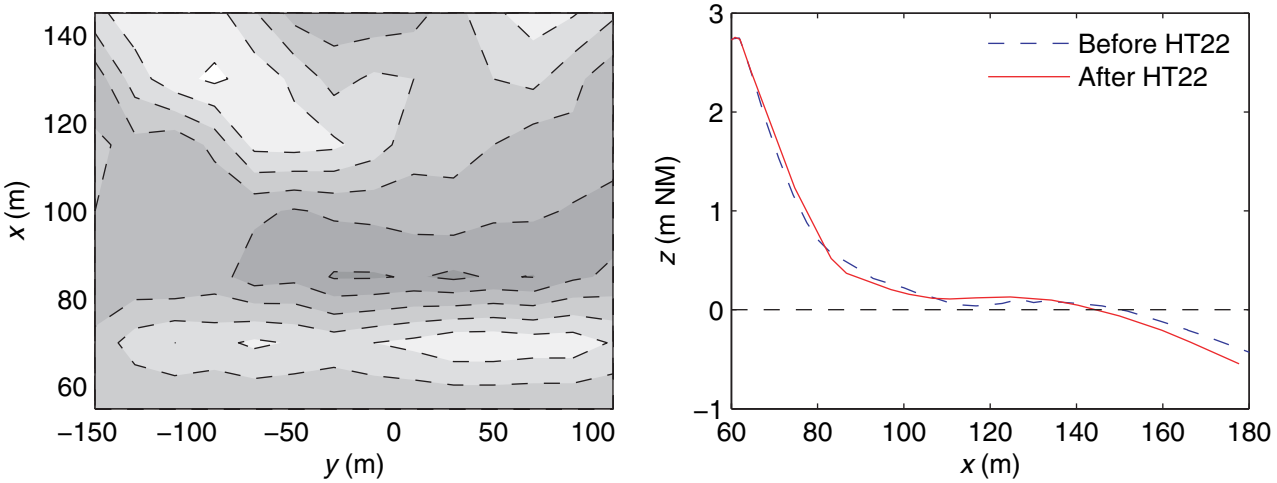

Fig. 6. Intertidal beach change that occurred during Tide 22. Left panel: three-dimensional change (measured at the sediment sampling locations) with the colour axis running from −0·1 m (grey; erosion) to +0·15 m (white; accretion). Right panel: intertidal beach profile before and after Tide 22 measured at the cross-shore transect $y = -20$ m.

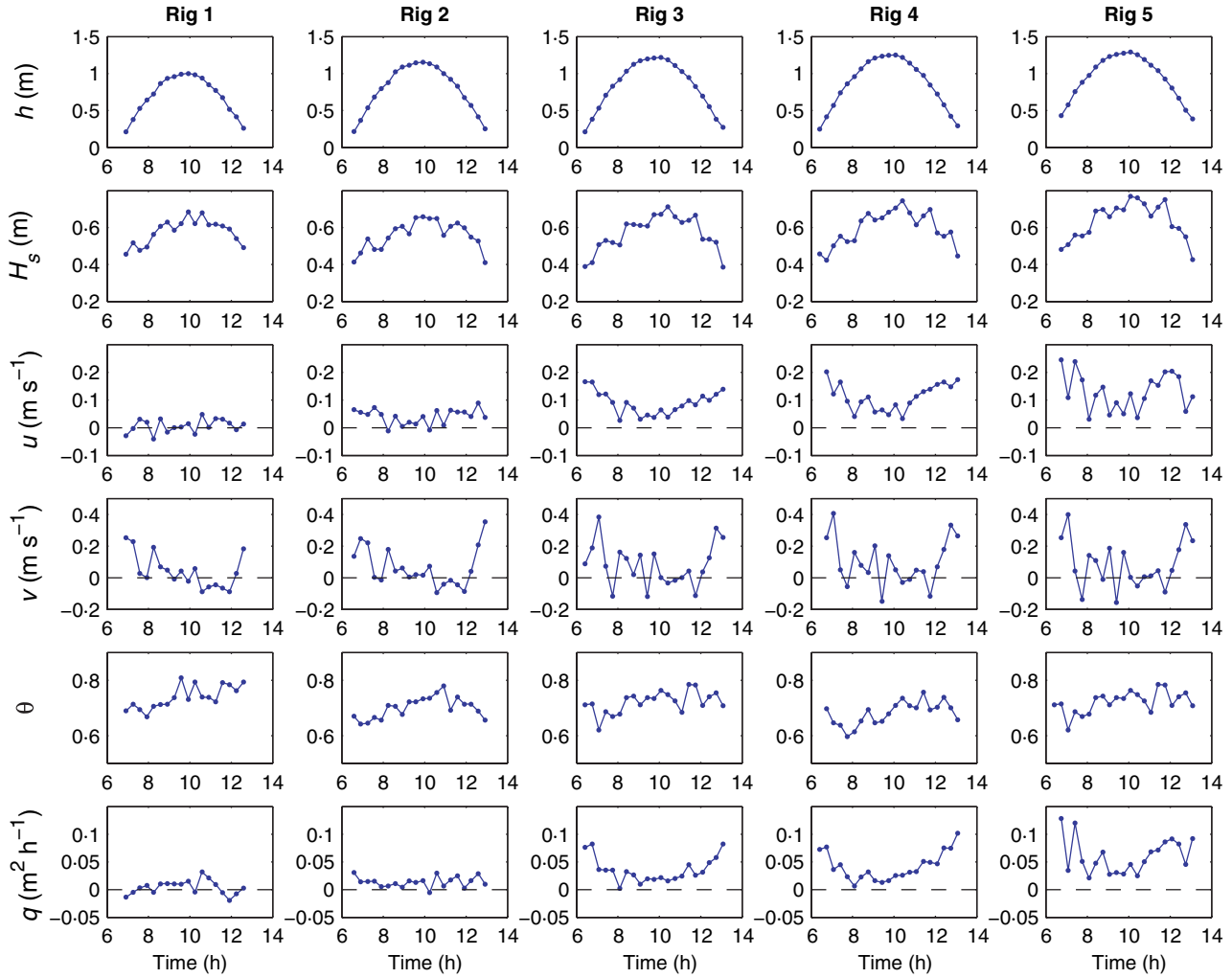

Fig. 7. Summary of the hydrodynamic conditions measured at the five instrument stations during Tide 22. From top to bottom: water depth h, significant wave height H_s, mean cross-shore current u, mean longshore current v, Shields parameter θ and total load sediment transport q computed according to Bailard (1981). The dots represent 20 min data segments.

respectively. The weakest currents are experienced during high tide when the mean flow velocities are almost insignificant. Bed shear stresses, parameterized by the Shields parameter θ, show an overall increase during the tidal cycle, probably related to an overall intensification of the wave forcing (refer to Fig. 5). The values for θ range from 0·6 to 0·8 and are indicative of energetic suspended sediment transport processes.

The net cross-shore sediment transport fluxes were computed using Bailard (1981). In agreement with the mean cross-shore flow data, the net sediment transport was in the onshore direction at all instrument locations, except at Rig 1, and the largest transport rates were found in shallow water and over the bar. It is further noted that the predicted onshore direction of the sediment transport across the bar surface, and the clear decrease in the transport rate from Rig 4 to Rig 2, corresponds to the observed landward bar migration. The predicted total onshore sediment transport during Tide 22 across the bar crest (Rig 4) is 0·25 m^3 per unit metre beach width.

The SRP data indicate that landward-migrating wave ripples were present at $x = 110$ m throughout Tide 22 (Fig. 8). The ripples were characterized by a height η and length λ of 6 and 60 cm, respectively. The steepness of the ripples η/λ is therefore 0·1, which classifies them as post-vortex ripples, as would be expected under the high bed shear stresses encountered ($\theta \approx 0{\cdot}7$). The migration rate of the ripples was 0·5 to 1 cm min^{-1}. The ripple geometry and dynamics during Tide 22 are

© 2007 The Authors. Journal compilation © 2007 International Association of Sedimentologists,

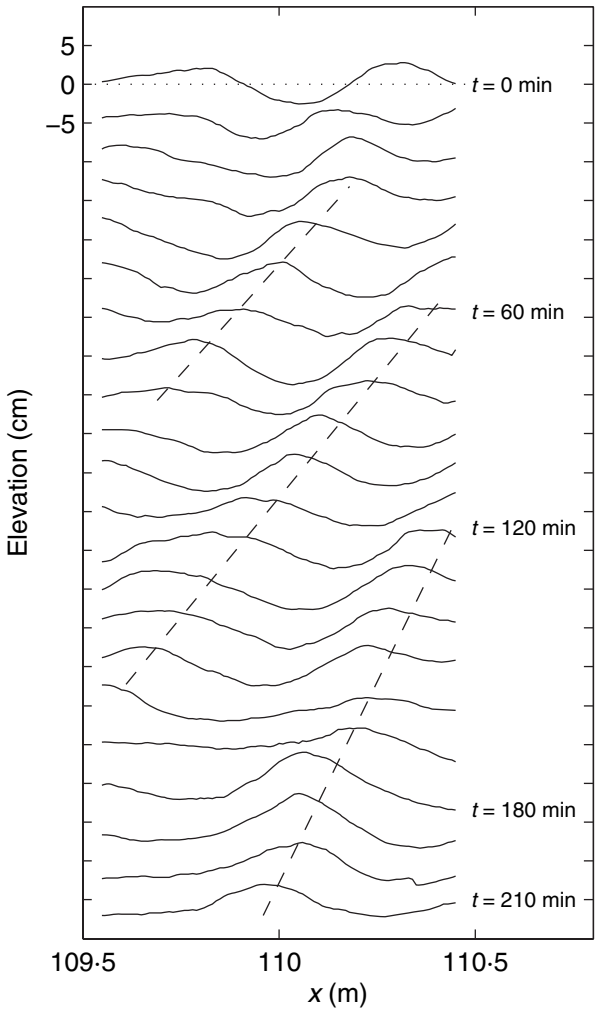

Fig. 8. Bed morphology at 10 min intervals recorded with the SRP at $x = 110$ m. The bed profiles have been vertically offset and clearly indicate landward migrating wave ripples. The dashed lines trace individual ripple crests over time.

very similar to those during the preceding tides and are described in more detail by Austin *et al.* (2007). The ripple migration rate M_r can be converted to a volumetric transport rate following Huntley *et al.* (1991) using $0{\cdot}5(1-p)\eta M_r$, where p is porosity. Assuming $p = 0{\cdot}4$, $\eta = 0{\cdot}06$ m and $M_r = 0{\cdot}5$ m h^{-1}, the resulting ripple transport rate is *ca* 0·01 m^3 h^{-1} (per metre beach width), which is of the same order as the predicted sediment flux according to the Bailard (1981) equation (Fig. 7). It is tempting to consider the ripple transport equivalent to the bedload transport rate but, under the high bed shear stresses encountered, it is probable that the migration of the ripples at least partly is due to suspended sediment transport (Masselink *et al.*, in press).

Spatial distribution in sediment size after Tide 22

The spatial distribution of the fall velocity parameters shows significant differences between the surface sediment and the sub-surface sediment (Fig. 9). Mean fall velocity ranges from 5 to 9 cm s^{-1} but, with the exception of a few patches on the upper beach (at $x = 85$ m), the surface sediment is consistently finer than the sub-surface sediment. This differentiation also is borne out by the mean fall velocity averaged over the whole measurement grid, which is 6·01 cm s^{-1} (SD = 0·28) for the surface sediment and 6·29 cm s^{-1} (SD = 0·57) for the sub-surface sediment. Overall, the upper beach is coarser than the lower beach. Both surface and sub-surface sediments are generally well to very well-sorted with sorting values ranging from $0{\cdot}2\psi$ to $0{\cdot}4\psi$ (the original sorting criteria of Folk & Ward (1957) are used here). The grid-averaged sorting for the surface and sub-surface sediment is $0{\cdot}27\psi$ (SD = 0·05) and $0{\cdot}30\psi$ (SD = 0·04), respectively. The spatial sorting pattern clearly indicates that the sediments from the trough region ($x = 100$ m) are the least well-sorted. The skewness of the sediments ranges from −0·4 to 0·8 and the differences between the surface and sub-surface sediment are very pronounced: the surface sediment is overwhelmingly positively skewed (fine-skewed) with a grid-averaged value of 0·44 (SD = 0·29), whereas the sub-surface sediments are negatively skewed (coarse-skewed) or symmetrical with a grid-averaged value of 0·04 (SD = 0·28). The least well-sorted sediments are characterized by the most negative skewness. Based on a two-tailed *t*-test, the surface and sub-surface sediment samples represent two different populations with respect to their mean sediment fall velocity and associated sorting and skewness at the 95% confidence level.

The difference between surface and sub-surface sediments is further exemplified by comparing the raw sediment fall velocity distributions (tails not removed) of the sediment collected at grid location $x = 145$ m and $y = -90$ m (Fig. 10). The mean and sorting of the surface and sub-surface sediments are comparable, but the surface sediment is positively skewed (0·66), whereas the sub-surface sediment is negatively skewed (−0·23). The difference in skewness between these two sediment types would have been even greater if the tails had not been removed prior to computing the moment statistics.

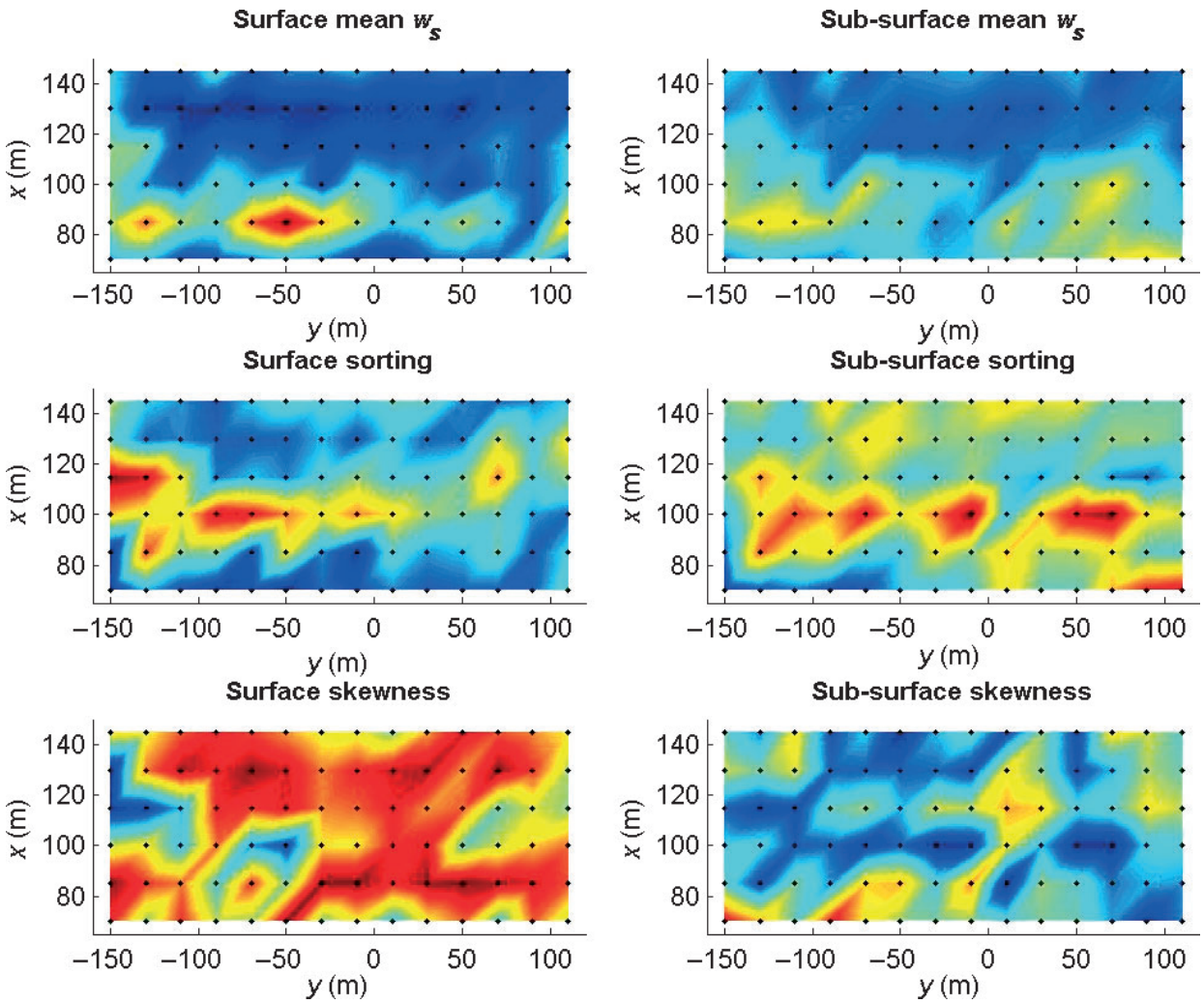

Fig. 9. Spatial trends in mean fall velocity w_s (upper panels), sorting (middle panels) and skewness (lower panels) for surface (left panel) and sub-surface sediments (right panels) after Tide 22. The colour axis runs from blue to red and represents 5 to 9 cm s^{-1} for the mean, 0·2 to 0·4ψ for the sorting and −0·4 to +0·8 for the skewness. The dots represent the sample locations.

Sediment trend analysis

Sediment trend vectors were derived for the GSTA and sorting model using both the surface and the sub-surface sediment, yielding four test cases (Fig. 11). There are few qualitative similarities between the trend vector pattern of the surface and sub-surface sediments. The agreement between the different trend models is also limited. At a cursory glance, none of the sediment trend patterns provide strong support for the observed onshore (lower panels in the diagram) and southward (left in the diagram) sediment transport.

The trend vectors were further analysed statistically for their significance. For each test case, the individual trend vectors were classified into four groups, depending on their direction: North (315° to 45°; longshore), East (45° to 135°; onshore), South (135° to 225°; longshore) and West (225° to 315°; offshore). The number of vectors in each class was then tabulated and compared with the observed sediment transport direction (Table 1). For each test case, the mean trend vector azimuth α was also computed through vector addition. Finally, a Rayleigh test was carried out to test for uniformity (or randomness/isotropy; Fisher, 1993).

The field observations and associated sediment transport predictions all indicate that the net direction of sediment transport during Tide 22 was East (onshore) and South (longshore). It is not possible to determine the relative importance of the cross-shore and longshore sediment transport

© 2007 The Authors. Journal compilation © 2007 International Association of Sedimentologists,

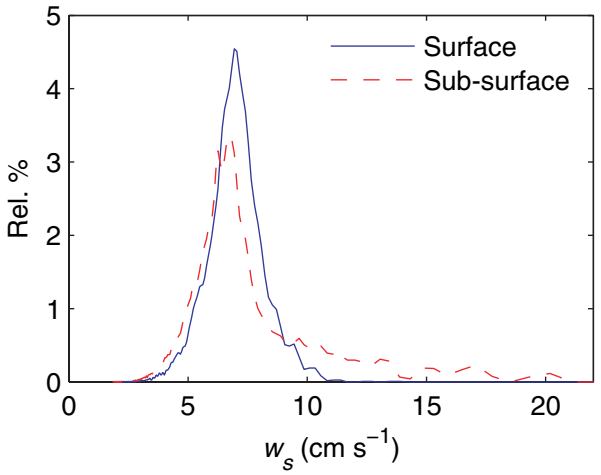

Fig. 10. Fall velocity distribution of surface and sub-surface sediment collected at grid location $x = 145$ m and $y = -90$ m. The mean, sorting and skewness for the surface sample are 5·29 cm s^{-1}, 0·25ψ and 0·70. The mean, sorting and skewness for the sub-surface sample are 5·69 cm s^{-1}, 0·27ψ and −0·04. The tails were removed from the fall velocity distribution prior to computing the moments, but the tails are included in the figure.

components, but the observed direction of net sediment transport must lie between 90° and 180°. There is no agreement between observed sediment pathways and those derived from sediment trend vectors (Table 1). The modal transport direction derived from the sediments is either North or West, and none of the mean angles of the trend vectors falls within the expected range. Moreover, the distribution of the trend vectors for two out of the four cases is random (Table 1).

Gao & Collins (1992) recommend averaging the trend vectors drawn from each sample point using its nearest neighbours over the characteristic transport distance D_{cr}, spatially filtering the vector field to remove noise and testing the significance of the resulting transport vectors. The trend vectors plotted in Fig. 11 have not been averaged, because both Asselman (1999) and Le Roux *et al.* (2002) strongly recommend against it, for averaging may lead to spurious results and a loss of information. Moreover, in the present study, averaging would bring together trend vectors from quite different beach sub-environments (bar and trough, trough and berm), which is inappropriate. However, to be consistent with the Gao & Collins (1992) approach, smoothing was carried out in order to test the significance of the results. This approach randomly redistributes each surface and sub-surface sample over the sampling grid a large number of times and, for each reshuffling, GSTA is conducted, resulting trend vectors smoothed over D_{cr} and the average length L of the transport vectors computed. The cumulative frequency distribution of L was then used to derive the 95% exceedance $L_{95\%}$. For the surface and sub-surface samples, $L_{95\%}$ was 0·32 and 0·31, respectively. The original data were also smoothed and L was computed for the surface ($L = 0{\cdot}40$) and the sub-surface samples ($L = 0{\cdot}32$). In both cases, $L > L_{95\%}$, implying that the transport vectors are significant at the 95% confidence level.

Application of hyperbolic model

The log-normal and log-hyperbolic models were fitted to the sediment fall velocity distributions of all surface and sub-surface sediment samples. Previous authors encountered difficulties in finding a stable numerical solution to the (highly nonlinear) optimization routine required to fit the log-hyperbolic model and reported failure rates of 25% to 30% (Fieller *et al.*, 1992; Sutherland & Lee, 1994). An unstable solution usually occurs when the curvature at the peak is undetectable due to relatively coarse resolution of the sediment data (Jones & McLachlan, 1989). However, for the present data set, a stable numerical solution always was found and this is attributed to the general symmetry in the measured distributions and to the high resolution provided by the settling tube method.

In agreement with other studies (Bagnold & Barndorff-Nielsen, 1980; Fieller *et al.*, 1992; Sutherland & Lee, 1994), it was found that the log-hyperbolic model fits the observed distributions very well and performs better than the log-normal model. The N_{crit} statistic (Eq. 7) was used to quantify the goodness-of-fit and clearly indicates the superior performance of the log-hyperbolic model (Table 2). The fall velocity distributions of the surface sediments are better described by the models than those of the sub-surface sediments.

Figure 12 plots the sediment data on the hyperbolic-shape triangle (refer to Fig. 4) and shows that neither surface nor sub-surface sediments are particularly normal in form and that, in general, the sub-surface sediments approximate a symmetrical log skew-Laplace distribution better than the surface sediments. Neither the surface nor the sub-surface sediments are particularly skewed, which is at odds with the findings of Hartmann & Christiansen (1992) who found con-

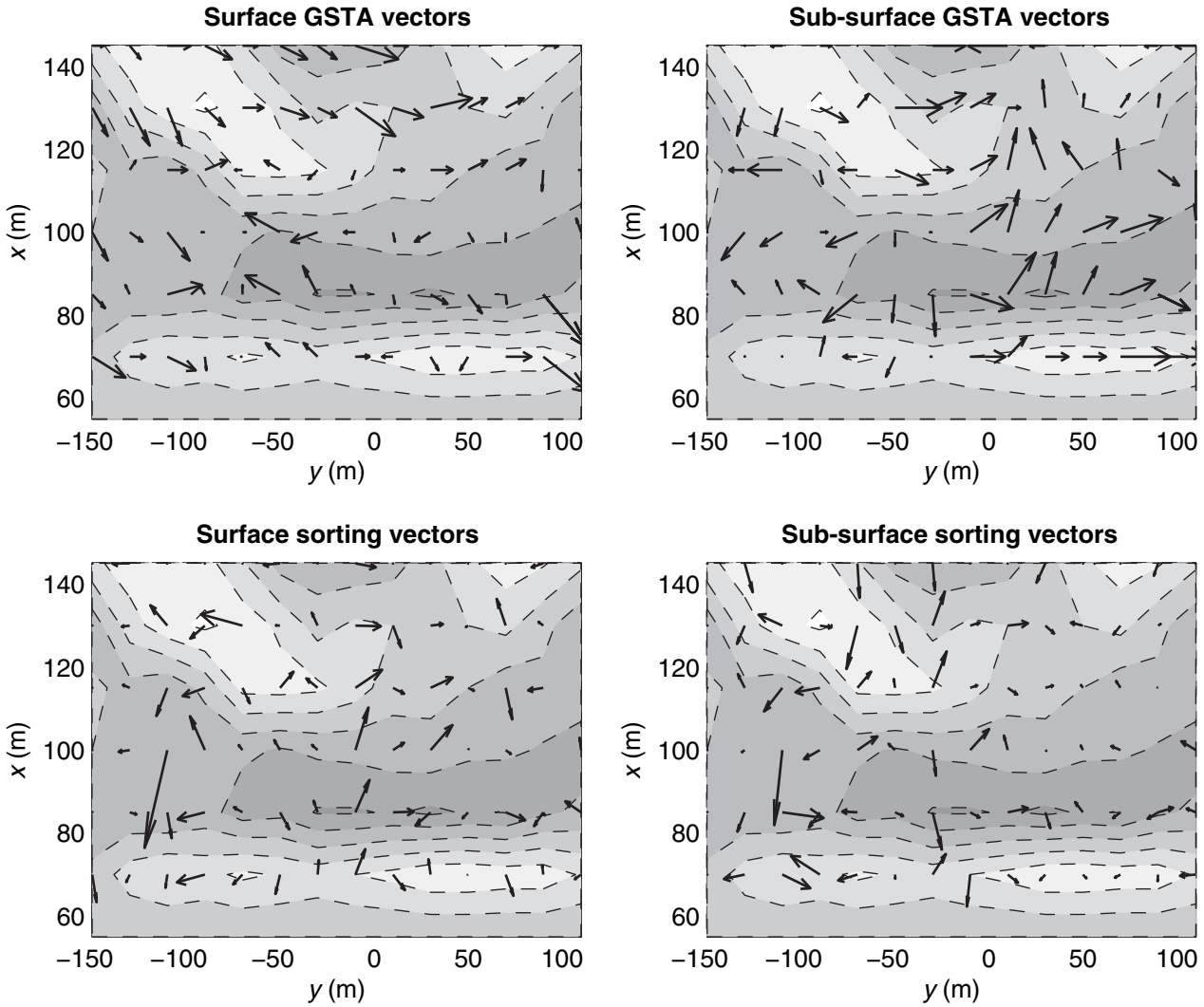

Fig. 11. Results of the sediment trend analysis superimposed on the morphological change that occurred during Tide 22. The colour axis runs from −0·1 m (grey) to +0·15 m (white). Trend vectors are shown, from top to bottom, for the GSTA model and the sorting model. The results using surface and sub-surface sediments are shown in the left and right panels, respectively.

Table 1. Summary of the trend vector analysis.

	% North	% South	% East	% West	α (°)	Randomness
Surface GSTA model	62	4	25	9	342	Random
Surface sorting model	11	10	23	40	21	Non-random
Sub-surface GSTA model	45	12	30	13	18	Non-random
Sub-surface sorting model	6	14	24	38	21	Random
Field observations	Net sediment transport is onshore (East) and longshore (South)					

sistent and marked negative skew in intertidal beach sands, and Sutherland & Lee (1994), who found consistent positive skew in mid-shore, upper-shore and back-shore, and strong negative skew for the lower foreshore. The data reported herein are similar to the symmetrical heavy-tailed beach sediments found by Lund-Hansen & Oehmig (1992). According to Fig. 12, the selective sorting model of Barndorff-Nielsen & Christiansen (1988) is unable to classify the surface or sub-surface sediments correctly into erosive or depositional environments. In fact, the vast majority of sediments in both cases plot in the depositional domain of the model.

© 2007 The Authors. Journal compilation © 2007 International Association of Sedimentologists,

Table 2. Average N_{crit} values quantifying the goodness-of-fit between the log-normal and log-hyperbolic models and the fall velocity distributions of surface and sub-surface sediments. The larger the value of N_{crit}, the better the fit.

	Log-normal	Log-hyperbolic
Sub-surface sediments	2100	9643
Surface sediments	2258	16544

DISCUSSION

This paper investigates the applicability of models that use spatial patterns in sediment characteristics to derive information on sediment transport processes in nearshore environments. The models tested include the GSTA model of Gao & Collins (1992) to determine sediment pathways and the hyperbolic triangle of Barndorff-Nielsen & Christiansen (1988) to distinguish between regions of accretion and erosion. The approach has been to collect comprehensive data on beach morphology, waves, tides, currents and sediment transport, complemented with sediment transport modelling, and compare these data and model results with the output of sediment trend models. The analysis is focussed on a single tidal cycle (Tide 22) and the

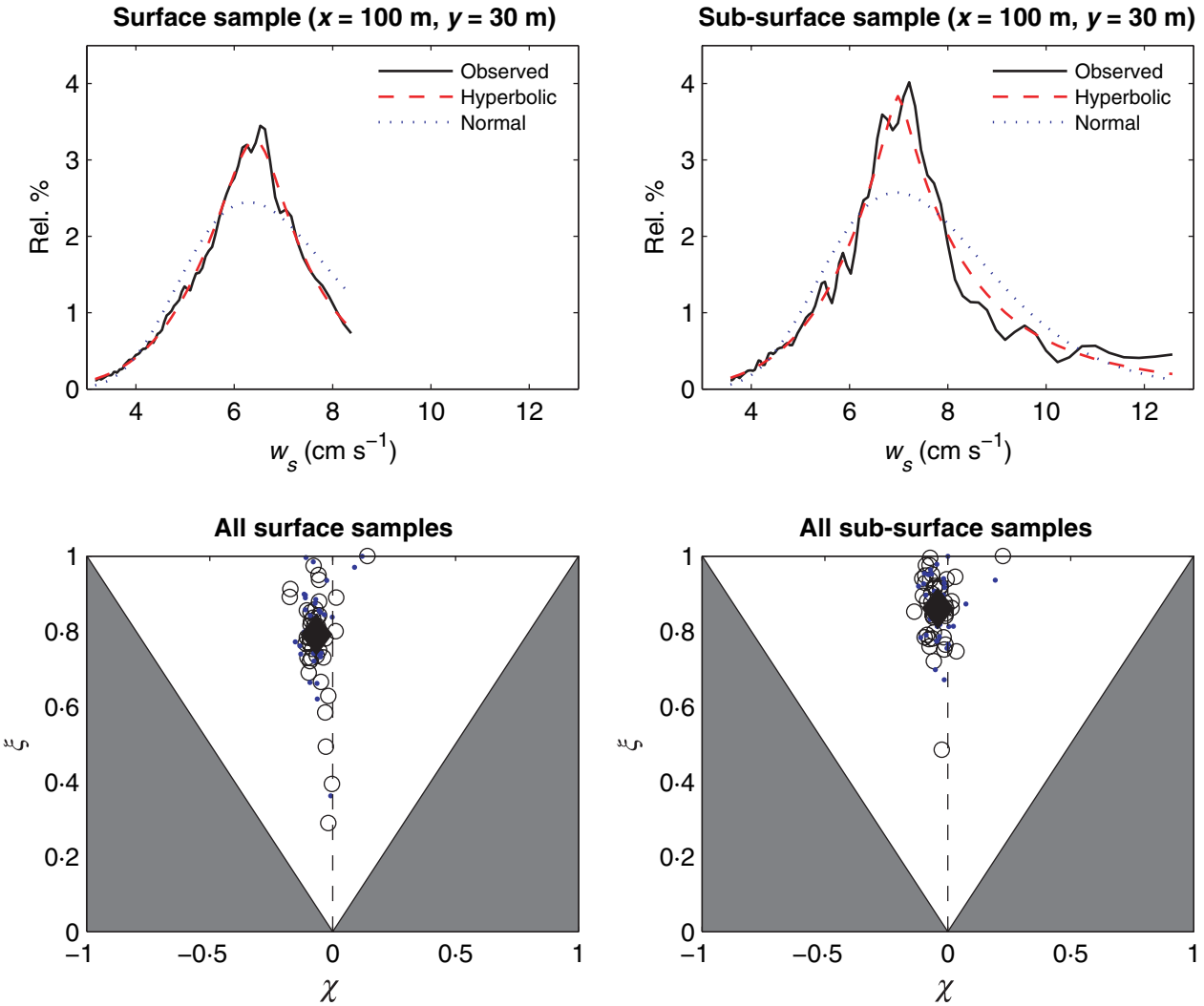

Fig. 12. Top panels: example comparison between measured fall velocity distribution (solid line) of surface (left panel) and sub-surface (right panel) sample collected at grid location $x = 100$ m and $y = 30$ m, and that fitted by log-hyperbolic (dashed line) and log-normal (dotted line) probability density functions. Bottom panels: [ξ, χ] position in the hyperbolic shape triangle for all surface (left panel) and sub-surface (right panel) sediment samples. The larger diamond denotes the centroid position. The depositional and erosional domains of the hyperbolic triangle are located, respectively, to the left and right of the vertical dashed line. Circles and dots represent samples from areas that displayed net accretion and erosion, respectively.

field observations clearly demonstrate that the sediment transport direction during this tide was predominantly in the onshore direction, possibly with an additional longshore (southward) component. Support for such a sediment transport pattern is provided by beach morphological surveys (upper beach accretion, onshore bar migration), hydrodynamic data (mean onshore current across the bar surface), sediment transport modelling [using the Bailard (1981) equation] and bedform observations (onshore-migrating wave ripples). Net onshore sediment transport is also in line with the longer-term morphological trend (berm build-up over a 10-day period) and suspended sediment transport measurements conducted during preceding tides (Austin *et al.*, 2007).

The sediment pathways were derived using the moment statistics of the fall velocity distribution of the sediment samples. The resolution of the sediment fall velocity data is much greater than that obtained using sieving; nevertheless, application of the GSTA model (Gao & Collins, 1992), and a slightly modified model solely based on sorting, was not very successful: no agreement was found between observed and derived sediment pathways, and significantly different sediment pathways were derived depending on whether surface or sub-surface sediment was used. In fact, the distribution of the directions of the sediment trend vectors was largely random. The log-hyperbolic model of Bagnold & Barndorff-Nielsen (1980) was fitted to the measured fall velocity distributions of the sediment samples to obtain fall velocity statistics. As expected, the log-hyperbolic model yielded an excellent fit to the data that was superior to fitting the log-normal model. However, plotting the relevant statistics (skewness and kurtosis) into the hyperbolic triangle (Barndorff-Nielsen & Christiansen, 1988) failed to correctly separate the sample locations into accretion and erosion: nearly all samples plotted in the deposition part of the triangle, while about half the samples were collected from areas experiencing erosion. The hyperbolic triangle model does not specify the thickness of the active sedimentary layer, therefore, the failure of the technique to correctly classify depleted and accreted sediments using the surface samples could be due to an inappropriate sample depth (cf. Martz & Li, 1997). However, because the model was tested using the surface and sub-surface sediments, the failure of the model to predict observed patterns of sedimentation is not due to sampling problems.

The present results are at odds with the findings of Pedreros *et al.* (1996), who applied the GSTA model to a beach very similar to that studied here (in fact, the two beaches are located only 30 km apart) and concluded that the model 'is extremely successful in a littoral environment'. There is no simple explanation for this discrepancy, but it should be pointed out that the two trend vector patterns obtained by Pedreros *et al.* (1996) (representing calm and storm conditions, respectively) were not analysed quantitatively (cf. Table 1), but merely interpreted by eye. Moreover, apart from a single fluorescent tracer deployment, no data (e.g. before-and-after beach surveys or wave/current observations) were available to indicate the actual net sediment transport directions.

Grain-size trend analysis has generally been applied to large-scale coastal systems, mainly estuaries, and it could be argued that the scale of the present investigation is too small for the method to be applicable. An explicit statement is neither made in McLaren & Bowles (1985), nor in Gao & Collins (1992) regarding the minimum spatial scale of analysis, but Le Roux and Rojas (in press) indicate that spacing between samples should probably be a minimum of 15 m. The sampling spacing used in the present investigation is not the smallest amongst GSTA studies: Rojas (2003) [see also Le Roux and Rojas, in press] obtained good results using a 10 m sample spacing across a 150×200 m grid for studying sediment pathways on a small lacustrine Gilbert-type delta.

The transport direction 'rules' defined by the GSTA model share an improvement in sorting in common, whereas coarsening/fining can co-vary with more negative/positive skewness. Sediment trend analysis, therefore, reaches a conclusion through the synthesis of a major premise (which asserts a universal truth regarding the relationship between transport direction and sorting), and a minor premise (which asserts a connection between transport direction and either size or skewness). As an expression of deductive reasoning (McLaren & Bowles, 1985), sediment trend analysis requires the premises to be true. While it is well-established that, in the direction of sediment transport, the sediment sorting improves due to selective sorting (Krumbein, 1938; Inman, 1949), there is less consensus with regard to the changes in the size and skewness. For example, beach sediments have been observed to both become finer (e.g. Self, 1977) and coarser (e.g. McCave, 1978) in the direction of

© 2007 The Authors. Journal compilation © 2007 International Association of Sedimentologists,

predominant transport. Skewness has been used to effectively discriminate between depositional environments (for example the use of bi-variate diagrams of sorting versus skewness to discriminate beach, river and dune deposits has been explored repeatedly; see Stewart, 1958; Friedman, 1967; Friedman & Sanders, 1978), yet shows little sensitivity to transport direction at the sedimentary sub-population level. McLaren & Bowles (1985) and Gao & Collins (1992) only consider cases FB− and CB+ for sediment trend analysis; however, net sediment transport pathways are not the only factor involved in generating spatial patterns in sediment characteristics and actually may be of subordinate importance when compared with other factors, especially in nearshore environments (Masselink, 1992, 1993).

The observed spatial pattern in sediment characteristics following Tide 22 can be explained *post-priori*, at least in part, on the basis of the morphological change, the cross-shore distribution of different morphodynamic zones across the intertidal profile, and a consideration of the sediment transport processes (Fig. 13). The swash-dominated, upper beachface ($x = 70$ m) experienced *ca* 10 cm accretion over the tidal cycle. Observations suggest that the sediments were advected into the swash zone by energetic breakers and turbulent bores acting just seaward of the swash zone, roughly over the region $x = 85$ to 100 m (cf. Jackson *et al.*, 2003). This area experienced erosion of 0·05 to 0·1 m and was characterized by the coarsest and least well-sorted sediments. Also, the sub-surface sediments here are the most coarse-skewed (negative skewness). The sediments in this region have the appearance of a lag deposit. Accretion of *ca* 0·1 m occurred on the bar crest at $x = 115$ m. The sediment characteristics here are average but, interestingly, the surface and sub-surface sediments are virtually identical. The sediments deposited on the bar surface were derived from the eroding seaward slope of the bar ($x > 130$ m). Here, the sub-surface sediments were relatively fine and well-sorted, but their coarse-skewed nature again suggests a lag-type deposit.

The spatial pattern in sediment characteristics across the intertidal zone partly can be explained by nearshore sediment transport processes, and some of the present results even can be seen to support the GSTA model tested here. For example, the onshore sediment transport from the intertidal trough to the upper beach (from $x = 100$ to 70 m), and from the seaward slope of the intertidal bar to the bar crest (from $x = 145$ to

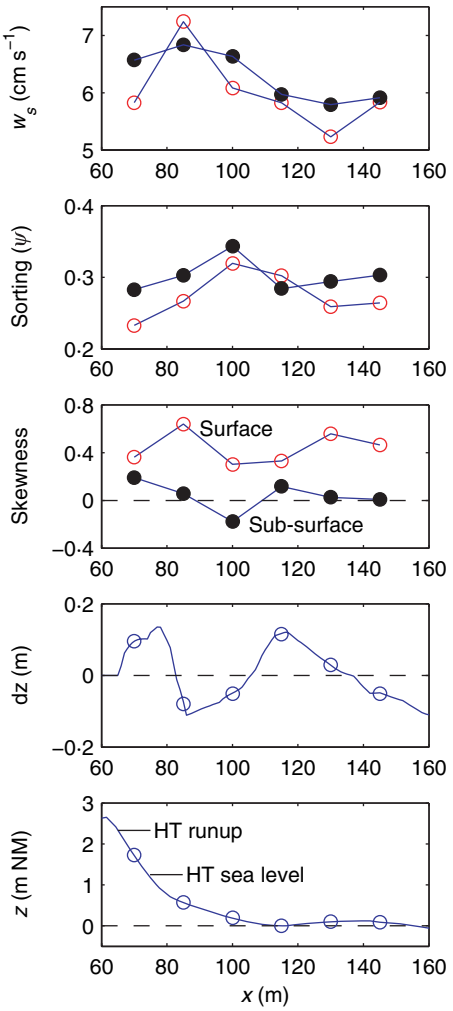

Fig. 13. From top to bottom: alongshore-shore averaged sediment fall velocity parameters (mean fall velocity w_s, sorting and skewness), morphological change during Tide 22 and beach morphology prior to Tide 22. The open and solid circles in the top three panels represent, respectively, the surface and sub-surface sediment; the open circles in the bottom two panels represent the sample locations.

115 m) can be interpreted as a CB+ sediment pathway (Fig. 13). However, deriving sediment pathways and erosion/accretion patterns in the intertidal zone of beaches solely on the basis of the sediments in a rigorous and statistically significant manner has proven impossible. Perhaps this is not surprising, considering the complexity of the nearshore sediment transport on tidal beaches, characterized by spatially varying and temporally varying wave processes (shoaling waves, breaking waves, swash), flows (cross-shore and longshore mean currents, orbital wave motion) and sediment fluxes (suspended load, bedload and sheet flow). It thus seems unrealistic to expect that sediment trend models would work

in situations other than under monotonically incrementing or fixed energy gradients, or at least where transport paths are uni-directional, or the residuals from a flow field show at least some consistent trend. Le Roux and Rojas (in press) noted that 'trend vectors obtained from grain-size parameters are not necessarily indicative of the direction of transport but depend on the environment of deposition'. On beaches, many different sub-environments (beachface, cusp, beach step, trough, rip channel, bar) are generally present within a relatively small area and the sediment variability arising from these secondary morphological features is likely to override any trends due to net sediment transport.

CONCLUSIONS

A large number of surface and sub-surface sediment samples were collected from a sandy beach and analysed using a settling tube. Moment analysis subsequently was used to derive the first three moments of the sediment fall velocity distribution (mean, sorting and skewness). The sub-surface sediments were usually characterized by the presence of a coarse 'tail', resulting in them being generally coarser, less well-sorted and more negatively skewed than the surface sediments. The moment statistics were used to derive sediment trend vectors according to the model of Gao & Collins (1992) and a model solely based on sorting. The sediment pathways derived from these models bore no relationship to the sediment transport observations and varied significantly depending on whether surface or sub-surface sediment samples were used. The log-hyperbolic model provides an excellent and much better fit to the sediment fall velocity distribution than the log-normal model. However, application of the hyperbolic triangle of Barndorff-Nielsen & Christiansen (1988), according to which sediments can be classified into accretion and erosion, was unsuccessful. The spatial distribution of sediment characteristics across the intertidal zone of the studied beach is considered mainly the consequence of the morpho-sedimentary history and the cross-shore distribution of the different morphodynamic zones across the intertidal profile (swash, trough and bar). The role of sediment pathways and whether the bed is accreting or eroding has only a limited effect on the sediment characteristics, rendering the use of sediment trend models in energetic nearshore environments questionable.

ACKNOWLEDGEMENTS

We would like to thank Tony Butt, Peter Ganderton, Tim Poate, Tim Scott, Jon Tinker and Emma Rendell for their assistance in the field. Further logistical support was provided by Nadia Sénéchal and her team from the University of Bordeaux. Isabelle Emmanuel assisted with some of the sediment analysis. This research was sponsored by the Natural Environmental Research Council through grant NER/A/S/2003/00553 'Cross-shore sediment transport and profile evolution on natural beaches (X-Shore project)' awarded to PR, GM and TOH.

REFERENCES

Ardhuin, F., Herbers, T.H.C., Watts, K.P., van Vledder, G.P., Jensen, R. and **Graber, H.** (2007) Swell and slanting fetch effects on wind wave growth. *J. Phys. Oceanogr.*, **37,** 908–931.

Asselman, N.E.M. (1999) Grain size trends used to assess the effective discharge for floodplain sedimentation, River Waal, the Netherlands. *J. Sed. Res.*, **69,** 51–61.

Austin, M.J., Masselink, G., O'Hare, T. and **Russell, P.E.** (2007) Relaxation time effects of wave ripples on tidal beaches. *Geophys. Res. Lett.*, **34,** L16606, doi: 10.1029/2007GL030696.

Bagnold, R.A. (1941) *The Physics of Blown Sands and Desert Dunes*. Methuen, London.

Bagnold, R.A. (1954) Experiments on a gravity-free dispersion of large solid spheres in a Newtonian fluid under shear. *Proc. Roy. Soc. London A*, **225,** 49–63.

Bagnold, R.A. and **Barndorff-Nielsen, O.** (1980) The pattern of natural size distributions. *Sedimentology*, **27,** 199–207.

Bailard, J.A. (1981) An energetics total load sediment transport model for a plane sloping beach. *J. Geophys. Res.*, **86,** 10938–10954.

Barndorff-Nielsen, O.E. (1977) Exponentially decreasing distributions for the logarithm of particle size. *Proc. Roy. Soc. London A*, **368,** 401–419.

Barndorff-Nielsen, O.E. and **Christiansen, C.** (1988) Erosion, deposition and size distributions of sand. *Proc. Roy. Soc. London A Math. Phys. Eng. Sci.*, **417,** 335–352.

Bascom, W.N. (1951) The relationship between sand size and beach-face slope. *Trans. Am. Geophys. Union*, **32,** 866–874.

Bauer, B.O. and **Allen, J.R.** (1995) Beach steps: an evolutionary perspective. *Mar. Geol.*, **123,** 143–166.

Blott, S.J. and **Pye, K.** (2001) GRADISTAT: a grain size distribution and statistics package for the analysis of unconsolidated sediments. *Earth Surf. Proc. Land.*, **26,** 1237–1248.

Bridge, J.S. (1981) Hydraulic interpretation of grain-size distributions using a physical model for bedload transport. *J. Sed. Petrol.*, **51,** 1109–1124.

De Melo Apoluceno, D., Howa, H., Dupuis, H. and Oggian, G. (2002) Morphodynamics of ridge and runnel systems during summer. *J. Coast. Res.*, **SI 36,** 222–230.

Fieller, N.R.J., Flenley, E.C. and **Olbricht, W.** (1992) Statistics of particle-size data. *Appl. Statist. J. Roy. Statist. Soc. C*, **41,** 127–146.

© 2007 The Authors. Journal compilation © 2007 International Association of Sedimentologists, *Sedimentology*, **55**, 667–687

Fisher, N.I. (1993) *Statistical Analysis of Circular Data*. Cambridge University Press, Cambridge.

Folk, R.L. and **Ward, W.C.** (1957) Brazos River bar: a study in the significance of grain size parameters. *J. Sed. Petrol.*, **27,** 3–26.

Friedman, G.M. (1967) Dynamic processes and statistical parameters compared for size-frequency distributions of beach and river sands. *J. Sed. Petrol.*, **37,** 327–354.

Friedman, G.M. and **Sanders, J.** (1978) *Principles of Sedimentology*. John Wiley, New York.

Gallagher, E.L., Elgar, S. and **Guza, R.T.** (1998) Observations of sand bar evolution on a natural beach. *J. Geophys. Res.*, **103,** 3203–3215.

Gao, S. (1996) A FORTRAN program for grain size trend analysis to define net sediment transport pathways. *Comput. Geosci.*, **22,** 449–452.

Gao, S. and **Collins, M.** (1991) A critique of the ''McLaren method'' for defining sediment transport paths – discussion. *J. Sed. Petrol.*, **61,** 143–146.

Gao, S. and **Collins, M.** (1992) Net sediment transport patterns inferred from grain-size trends, based upon definition of transport vectors. *Sed. Geol.*, **81,** 47–60.

Gibbs, R.J., Matthews, M.D. and **Link, D.A.** (1971) The relationship between sphere size and settling velocity. *J. Sed. Petrol.*, **44,** 7–18.

Greenwood, B. and **Davidson-Arnott, R.G.D.** (1972) Textural variations in sub-environments of the shallow water wave zone, Kouchibouguac Bay, New Brunswick. *Can. J. Earth Sci.*, **9,** 679–688.

Hartmann, D. and **Christiansen, C.** (1992) The hyperbolic shape triangle as a tool for discriminating populations of sediment samples of closely connected origin. *Sedimentology*, **39,** 697–708.

Hughes, M.G., Keene, J.B. and **Joseph, R.G.** (2000) Hydraulic sorting of heavy-mineral grains by swash on a medium-sand beach. *J. Sed. Res.*, **70,** 994–1004.

Huntley, D.A., Amos, C.L., Williams, J.J. and **Humphery, J.D.** (1991) Estimating bedload transport on continental shelves by observations of ripple migration – an assessment. In: *Euromech 262 – Sand Transport in Rivers, Estuaries and the Sea* (Eds R. Soulsby and R. Betess), pp. 17–24. Balkema, Rotterdam.

Inman, D.L. (1949) Sorting of sediments in the light of fluid mechanics. *J. Sed. Petrol.*, **19,** 51–70.

Inman, D.L. (1953) Areal and seasonal variations in beach and nearshore sediments at La Jolla, California. *US Army Corps of Engineers, Beach Erosion Board Technical Memo*, **39,** Fort Belvoir, VA, USA.

Jackson, N.L. and **Nordstrom, K.F.** (1993) Depth of activation of sediment by plunging breakers on a steep sand beach. *Mar. Geol.*, **115,** 143–151.

Jackson, N., Masselink, G. and **Nordstrom, K.F.** (2003) The role of bore collapse and local shear stresses on the spatial distribution of sediment load in the uprush of an intermediate-state beach. *Mar. Geol.*, **203,** 109–118.

Jones, P.N. and **McLachlan, G.J.** (1989) Modelling mass-size particle data by finite mixtures. *Commun. Statist. Theory Meth.*, **18,** 2629–2646.

Krumbein, W.C. (1938) Size-frequency distributions of sediments and the normal phi curve. *J. Sed. Petrol.*, **8,** 84–90.

Le Roux, J.P. (1994) An alternative approach to the identification of net sediment transport paths based on grain-size trends. *Sed. Geol.*, **94,** 97–107.

Le Roux, J.P. and **Rojas, E.M.** (in press) Sediment transport patterns determined from grain size parameters: overview and state of the art. *Sed. Geol.*, doi: 10.1016/j.sedgo.2007.03.014.

Le Roux, J.P., O'Brien, R.D., Rios, F. and **Cisternas, M.** (2002) Analysis of sediment transport paths using grain size parameters. *Comput. Geosci.*, **28,** 717–721.

Lucio, P.S., Bodevan, E.C., Dupont, H.S. and **Ribeiro, L.V.** (2006) Directional kriging: a proposal to determine sediment transport. *J. Coast. Res.*, **22,** 1340–1348.

Lund-Hansen, L.C. and **Oehmig, R.** (1992) Comparing sieve and sedimentation balance analysis of beach, lake and eolian sediments using log hyperbolic parameters. *Mar. Geol.*, **107,** 139–147.

Martz, L.W. and **Li, L.** (1997) Grain-size analysis of surface material under wind erosion using the effective surface concept. *Earth Surf. Proc. Land.*, **22,** 19–29.

Masselink, G. (1992) Longshore variation of grain size distributions along the coast of the Rhone delta, Southern France: a test of the ''McLaren model''. *J. Coast. Res.*, **8,** 286–291.

Masselink, G. (1993) Longshore variation of grain size distribution along the coast of the Rhone Delta, Southern France: a test of the ''McLaren model'' – Reply. *J. Coast. Res.*, **9,** 1142–1145.

Masselink, G. and **Short, A.D.** (1993) The effect of tide range on beach morphodynamics and morphology – a conceptual beach model. *J. Coast. Res.*, **9,** 785–800.

Masselink, G., Auger, N., Russell, P. and **O'Hare, T.** (2006) Short-term morphological change and sediment dynamics in the intertidal zone of a macrotidal beach. *Sedimentology*, **45,** 39–53.

Masselink, G., Austin, M., O'Hare, T. and **Russell, P.** (in press) Geometry and dynamics of wave ripples in the nearshore zone of a coarse sandy beach. *J. Geophys. Res.*, doi: 10.1029/2006jc003839.

McCave, I.N. (1978) Grain size trends and transport along beaches: example from eastern England. *Mar. Geol.*, **28,** M43–M51.

McLaren, P. (1981) An interpretation of trends in grain-size measures. *J. Sed. Petrol.*, **51,** 611–624.

McLaren, P. and **Bowles, D.** (1985) The effects of sediment transport on grain-size distributions. *J. Sed. Petrol.*, **55,** 457–470.

McLaren, P., Hill, S.H. and **Bowles, D.** (in press) Deriving transport pathways in a sediment trend analysis (STA). *Sed. Geol.*, doi: 10.1016/j.sedgeo.2007.03.014.

Miller, R.L. and **Ziegler, J.M.** (1958) A model relating dynamics and sediment pattern in equilibrium in the region of shoaling waves, breaker zone, foreshore. *J. Geol.*, **66,** 417–441.

Mothersill, J.S. (1969) A grain size analysis of longshore-bars and troughs, Lake Superior, Ontario. *J. Sed. Petrol.*, **39,** 1317–1324.

Pedreros, R., Howa, H.L. and **Michel, D.** (1996) Application of grain size trend analysis for the determination of sediment transport pathways in intertidal areas. *Mar. Geol.*, **135,** 35–49.

Poizot, E., Mear, Y., Thomas, M. and **Garnier, S.** (2006) The application of geostatistics in defining the characteristic distance for grain size trend analysis. *Comput. Geosci.*, **32,** 360–370.

Robson, D., Fieller, N. and **Stillman, E.** (1997) *ShefSize. Department of Probability and Statistics*. University of Sheffield, Sheffield, UK.

Rojas, E.M. (2003) *Determinación de vectores de transporte utilizando información exclusivamente granulométrica: aplicación al delta tipo Gilbert, del rio de Pescado, Llago*

Llanquihue, X Region, Chile. MSc Thesis (unpublished). Universidad Chili.

Self, R.P. (1977) Longshore variation in beach sands, Nautla area, Veracruz, Mexico. *J. Sed. Petrol.*, **47,** 1437–1443.

Short, A.D. (1991) Macro-meso tidal beach morphodynamics – an overview. *J. Coast. Res.*, **7,** 417–436.

Slingerland, R.L. (1977) Effects of entrainment on hydraulic equivalence relationships of light and heavy minerals in sands. *J. Sed. Petrol.*, **47,** 753–770.

Soulsby, R. (1997) *Dynamics of Marine Sands*. HR Wallingford, Thomas Telford, London, UK.

Stewart, H.B. (1958) Sedimentary reflections on depositional environments in San Migue Lagoon, Baja, California, Mexico. *Bull. Am. Assoc. Petrol. Petrol. Geol.* **42,** 2567–2618.

Sutherland, R.A. and **Lee, C.T.** (1994) Application of the log hyperbolic distribution to Hawaiian beach sands. *J. Coast. Res.*, **10,** 251–262.

Swart, D.H. (1974) A schematization of onshore-offshore transport. *Proceedings 14th International Conference on Coastal Engineering ASCE*, pp. 884–900, Copenhagen, Denmark.

Thornton, E.B. and **Guza, R.T.** 1982) Energy saturation and phase speeds measured on a natural beach. *J. Geophys. Res.*, **97,** 9499–9508.

Tinker, J., Russell, P., Masselink, G., O'Hare, T., Butt, T., Ganderton, P. and **Gallagher, E.** (2006) Cross-shore sediment transport and profile evolution on natural beaches: The X-SHORE Project. *Proceedings 30th International Conference on Coastal Engineering ASCE*, San Diego, CA, USA.

Turner, I.L. (1995) Simulating the influence of groundwater seepage on sediment transported by the sweep of the swash zone across macro-tidal beaches. *Mar. Geol.*, **125,** 153–174.

Van Houwelingen, S.T., Masselink, G. and **Bullard, J.E.** (2006) Characteristics and dynamics of multiple intertidal bars, north Lincolnshire, England. *Earth Surf. Proc. Land.*, **31,** 428–443.

Van Rijn, L.C. (1993) *Principles of Sediment Transport in Rivers, Estuaries and Coastal Seas*. Aqua Publications, Amsterdam.

Wyrwoll, K.H. and **Smyth, G.K.** (1985) On using the log-hyperbolic distribution to describe the textural characteristics of eolian sediments. *J. Sed. Petrol.*, **55,** 471–478.

Manuscript received 30 April 2007; revision accepted 14 September 2007

© 2007 The Authors. Journal compilation © 2007 International Association of Sedimentologists, *Sedimentology*, **55**, 667–687